Indian J. Phys. **66B** (5 & 6), 537 – 548 (1992)

Expansion hydrodynamics of laser heated and imploded microshell

Yu A Zakharenkov, A S Shikanov, I G Lebo, V B Rozanov
P N Lebedev, Physical Institute, USSR Academy of Sciences, USSR

T V Mishchenko, G V Shpatakovskaya and M V Keldysh
Institute of Applied Mathematics, USSR Academy of Sciences, USSR

Z Ahmad and T A Hall
University of Essex, U K

Abstract : New diagnostic method of laser implosion of microshell targets based on time-of-flight mass-spectrometer of neutral atoms is described. Experiments have been conducted at 12-beam laser facility "Vulcan" in Rutherford Appleton Laboratory on implosion of high aspect ratio glass shell targets. Theoretical analysis and numerical simulations of neutral atom velocity spectrum gave evidence of different physical processes of atom emission such as cumulative jet and fuel mixing as well as shock wave formation due to shell deceleration in plasma corona. Application of neutral atom pinhole camera has allowed to observe emitting areas around the target.

Keywords : Microshell, expantion hydrodynamics, laser implosion, time-of-flight mass-spectrometry

PACS Nos. : 52.50. Jm, 07.75. + h

1. Introduction

In laser heating and implosion of microshell [1] one can distinguish two periods in hydrodynamics of target material expansion. The first period lasts until the laser pulse is over, and its duration usually is not longer than implosion time. As the result of laser interaction high temperature (1 keV and more) plasma is produced on the target surface. The density of multicharged ions is of $10^{20} - 10^{22}$ cm^{-3}, their expansion velocities– (4–8). 10^7 cm/s. As was shown in theory [2,3] and confirmed experimentally [4–6], the probability of ion recombination to neutral atom state in the course of plasma expansion is extremely small. The registration of neutral atoms is possible only in the slow part of particle velocity distribution (velocity less than 4.10^7 cm/s). Hence hydrodynamics research (mass ablation rate, ablation pressure) of laser heated target is widely based on ion mass-spectrometer methods [7].

The second particle emission period starts from the moment of microshell implosion (laser pulse is over by this time, no laser heating). Characteristic expansion velocities and charge composition of particle flow depend on the imploded target parameters. At the densities of ρ_s = 10-100 g/cm^3 and temperatures of T_s = 10-100 eV the pressure in the microshell centre is $P_{imp} \geq 10^9$ bar [8]. One can consider these values as initial conditions for particle acceleration. High density and low temperature provide conditions for fast recombination of low charged ions in the very beginning of their expansion motion.

The asymptotic velocities of such atoms $V \propto (P_{imp}/\rho_{imp})^{1/2}$ in the contrast to the hot plasma corona ions do not exceed the maximal implosion velocity of the shell $u_s \approx (1\text{-}3).10^7$ cm/s. Hence time-of-flight measurements are the most reliable because of temporal separation of plasma and imploded shell atoms. Application of electrostatic ion deflector on the path of flight allows only neutral atoms reach the detector (as well as X-rays coming much earlier).

In the case when considerable part of microshell mass is imploded increasing of density and preheating control results in increasing of ion recombination degree, so neutral atom portion in particle flow noticeable [9]. As was shown in numerical simulations [10], this part may exceed 90% of imploded microshell mass. Therefore one comes to conclusion on possibility of developing of particle diagnostics imploded shell target : determination of hydrodynamics efficiency of implosion, residual microshell mass and other important parameters.

In this paper we discuss the measurement results of two types on time-of-flight neutral particle detectors : secondary emission electron multiplier and gated microchannel plate pinhole camera, which were used in implosion experiments on laser facility "Vulcan" [11]. It should be noted that in the case of high aspect ratio shells compression is not ablative, so residual mass has higher ionization degree. One of the aims of conducted experiments was investigation of influence of laser uniformity of target irradiation, changed with different types of laser beam focusing, on neutral particle velocity distribution.

2. Experimental layout

Experiments have been conducted at 12-beam laser facility "Vulcan" in Rutherford Appleton Laboratory on implosion of high aspect ratio glass shell targets. Scheme of experiment is shown in the Figure 1.

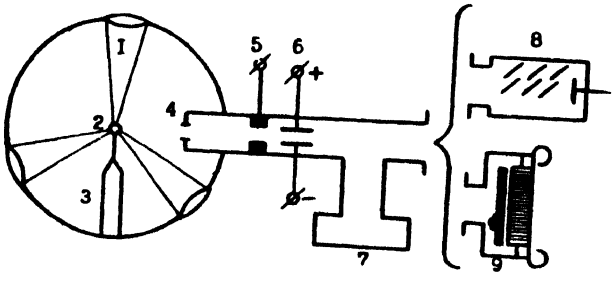

Figure 1. The scheme of experiment : (1)—laser beam, (2)—target, (3)—target support stalk, (4)—pinhole holder, (5)—ion collector, (6)—ion deflector, (7)—vacuum pumping, (8)—secondary electron multiplier, (9)—microchannel plate neutral particle beam image detector.

Laser energy in these experiments was in the range of 500-800 J in the pulse of 0.6 ns duration at the wavelength 0.53 μm. Targets used in these experiments were DT and D_2 filled glass high aspect ratio shells with diameter of 500-700 μm wall-thickness of 0.75 - 1.3 μm. A few laser shots were produced with the empty thick (2.3 μm) glass and plastic (up to 11 μm wall-thickness) shells. Experiments were aimed to investigate the effects of different focusing conditions, *e.g.* influence of random phase plates inserted in the laser beams on implosion parameters [12].

Diagnostics used in the experiments included X-ray detectors (streak camera, crystal spectrograph, pin-hole cameras), neutron and α-particle counters [13] and neutral particle detectors [14]. The viewing axis of neutral particle detection channel was located in the middle of equisided triangle formed by nearest three laser beams (at the angle of 30° to the laser beam axis). Chosen arrangement made possible to detect particles from the "cold" area of target, surrounded by the three "hot" spots.

The neutral particle detector (secondary electron multiplier or micro channel camera) was arranged at the distance L = 110 cm from the target. For plasma ion velocity distribution monitoring ion collector at the distance 90 cm was used. Behind the ion collector electrostatic ion deflector (plane capacitor with output slit) was placed. Pinholes with diameter 50 or 100 μm can be arranged inside vacuum chamber at the distance 5 – 25 cm from the target. For elimination the X-ray exposure of high sensitive microchannel plate the method of time gated feeding voltage was applied [15]. Images of neutral particle sources were registered with photographic film in tight contact with fiber optics screen.

3. Experimental results

The typical signal traces of secondary electron multiplier, obtained in the nonuniform and uniform target irradiation laser shots, are presented in the Figure 2. Velocity range of detected atoms is (0.75 - 4.4) × 10^7 cm/s. Structure of the each signal can be analyzed while

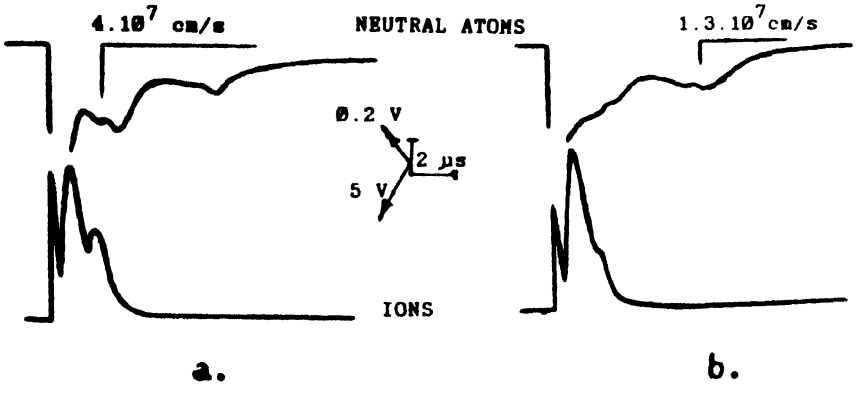

Figure 2. Oscilloscope traces of ion and neutral atom detectors : (a)— nonuniform irradiation laser shot; (b)— laser shot with random phase plates.

comparing with the signal of ion collector (lower trace). The first ion maximum (trace on Figure 2a) corresponds to velocity of 8.2 × 10^7 cm/s and consists of the ions, emitted from the "hot" spots on the target surface.

The second ion peak has velocity 3.85×10^7 cm/s and probably originated from "cold" target area. The characteristic feature of second ion peak is a long low velocity tail (up to 1.5×10^7 cm/s).

Comparison of neutral and ion traces allows us to divide neutral particle signal by two parts : (I) — fast atoms, appeared due to recombination of ions from "cold" area (ions from "hot" areas did not recombine because of high initial temperature), (II) — slow atoms of residual target mass (velocity range 0.7 - 1.5 $\times$ 10^7 cm/s). The form of neutral signal had visible unreproducible character, but depending on the type of focusing. From Figure 2 it can be noted that non uniform irradiation produce more fast atoms with velocity up to 4.10^7 cm/s and less structure signal in the range of slow atoms (velocity of 1.3×10^7 cm/s). Uniform irradiation neutral particle pulse was characterised by faster decreasing voltage after slow atoms peak.

Registration of pinhole images of neutral particle source provided more important data on explanation of atom spectra obtained. In Figure 3 the pinhole image of plastic shell with diameter 266.4 μm and wallthickness 9.2 μm is presented. The time gating was corresponded to velocity range of (1.3 - 1.8) $\times$ 10^7 cm/s. It is clear that registered slow atoms came not only from target but from its support stalk as well. This may be the consequence of radiation heating or conduction from the target, and the effects of focused laser radiation propagating aside the target. Special type of image, obtained in this particular shot, correlate with small shell diameter and relatively high laser energy (E_{las} = 748 J). In Figure 3b photometric trace of axial cross section of target image is presented. It is possible to observe spatial intensity structure of 150 μm size, which related to spatial resolution of pin-hole camera (100 μm diameter of pin-hole aperture, magnification of 10).

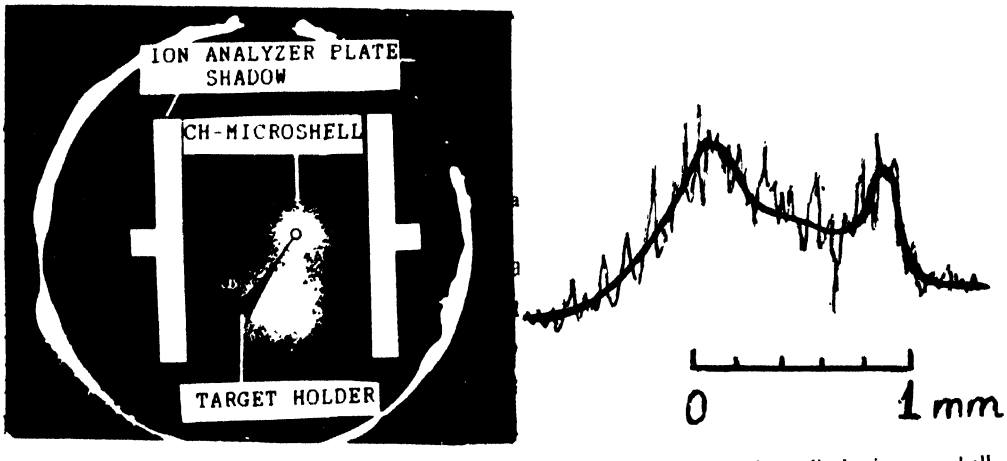

Figure 3. Pinhole image of neutral particle emission in shot with small plastic microshell diameter 266.4 μm.

The method of neutral particle emission imaging has a great importance for interpretation of time-of-flight data. First, we can count the pixel area density in recorded

image (for the case of Figure 3 it was about 50 pix/mm^2). This value provide the basic information on registration efficiency and secondary electron emission coefficient, which was used for evaluating of slow atom velocity spectrum. Secondly, we should check the dimensions of shell and laser energy each time when get some unusual feature in spectrum.

4. Discussion

Numerical simulations:

Processes of laser heating, implosion and expansion of microshell were investigated with numerical simulation on one-dimensional code "Diana" [10,16]. Laser pulse was approximated with gaussian shape:

$$dE/dt = dE_0/dt \exp\left\{-4\ln 2\,[(t-t_0)/\tau]^2\right\}, \quad (1)$$

where E_0—absorbed laser energy, t_0—time of pulse maximum, τ—full width on half maximum (FWHM). The values of E_0 were taken from ion collector measurements [7], usually absorbed energy was in the range of 300-350 J. In the Table 1 we present the computed parameters at the implosion time of glass microshell with initial diameter 592 μm and wall-thickness 1.1 μm, filled with DT gas (initial density $\rho_{DT} = 4.64 \times 10^{-4}$ g/cm^3). There were three variants of simulation ($t_0 = 1.2$ ns in each variant) : (1) $E_0 = 300$ J, $\tau = 0.6$ ns; (2) $E_0 = 300$ J, $\tau = 0.84$ ns; (3) $E_0 = 350$ J, $\tau = 0.84$ ns. Changing the E_0 and τ reinvestigated the influence of flux density and pulse width on particle expansion parameters.

Average velocity of microshell implosion u_{av} is determined as $u_{av} = R_0 / t_{imp}$, M_{sh} is mass of unblated shell part (initial shell mass $M_0 = 3.11$ μg, the mass of DT fuel is $M_g = 0.05$ μg), ρ_{sh}, T_{sh}, ρ_{DT}, T_{DT} are mass averaged density and temperature of shell and fuel respectively, Y_n is neutron yield.

Table 1. Computed parameters at the implosion time of glass microshell.

Variant	t_{imp}	u_{av}	M_{sh}	ρ_{sh}	T_{sh}	ρ_{DT}	T_{DT}	Y_n
#E_0/τ	ns	km/s	μg	g/cm^3	eV	g/cm^3	keV	10^9
1 300/0.6	2.23	134	0.75	6.3	327	1.16	1.72	4.6
2 300/.84	2.31	128	0.88	15.0	246	1.85	1.4	2.4
3 350/.84	2.16	137	0.75	10.6	335	1.77	1.62	5.4

It is obvious, that increasing of pulse width (var. 2) is equivalent to decreasing of flux density, which leads to reduction of u_{av} and ablated mass and consequently results in reduction of fuel temperature and neutron yield, but the densities of imploded shell and fuel have noticeable increase. Such sensitive behaviour of high aspect ratio shell implosion parameters on laser pulse characteristics should be taken into consideration while discussing experimental data.

After implosion time, when practically all imploded substance was heated and ionized high density core expansion in low density plasma corona begins and partial recombination of Si, O, D and T ions occurs. In Figure 4 velocity distributions of neutral atoms calculated in

Var. 1 and 2 are presented. It should be noted, that the expansion time for displayed distributions is corresponded to 10 ns. It was limited becaues of time consuming problems with numerical simulation up to 1-10 μs range. Nevertheless neutral atom distributions obtained are very close to the final due to very fast "freezing" effect in low density expanding plasma corona [3], so we may assume that after the period of 10 ns average ion charge is constant. Simulation of Var. 2 produced no measurable number of neutral Si and O atoms.

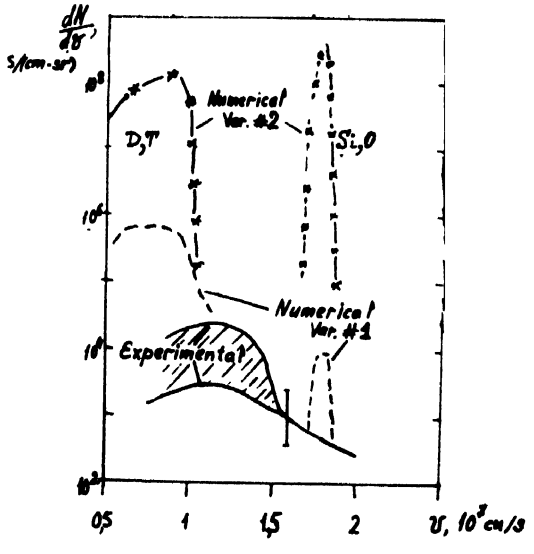

Figure 4. Numerically calculated atom velocity distributions at the expansion time 10 ns for variants (1) and (2), corresponding to Table 1.

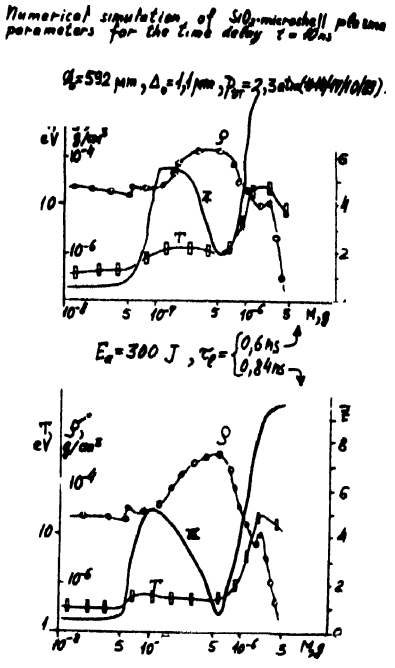

Figure 5. Radial distributions of expanding shell mass density (ρ), electron temperature (T_e) and mass averaged ion charge (z) for the expansion time 10 ns (a) — Var. 1, (b) — Var. 2 of Table 1. Vertical broken line is shell-fuel interface, M_0 is initial terget mass.

In Figure 5 radial distributions of mass density, electron temperature and mass averaged ion charge are presented. There is obvious contrast with the analogous distributions, calculated for experiment at the laser facility "Delfin" [10], where thick microshell were used (so residual target mass was much more larger and up to 90% of shell ions recombined to neutral state). From Figure 5 it is possible to integrate neutral atom partition in particle expansion flow. This value is near to 1-3% of the compressed target mass and the most part of neutral particles is represented by DT fuel in low velocity band of distribution.

Experimental atom distributions :

For derivation of atom velocity distribution from experimentally registered detector signals following relation similar to the case of ion collector was used :

$$dN/dv = L \times I/(k \times e \times \Gamma \times v^2 \times \Omega), \quad (2)$$

where L is the distance from the target, I is detector current, k is the amplification of secondary electron emission of detector (with the coefficient Γ), Ω is the solid angle. As we mentioned early particle pin-hole imaging was of great importance for evaluation of $\Gamma(v)$ function (only sparse literature, *e.g.* [17], can be available). For the velocity range under investigation it was assumed $\Gamma(v) \alpha v^2$.

In the Figure 6 slow atom velocity spectra are presented. They look very similar, and it is possible to approximate all of them with the curve :

$$dN/dv = N_0 \times \exp(-v/v_0), \quad (3)$$

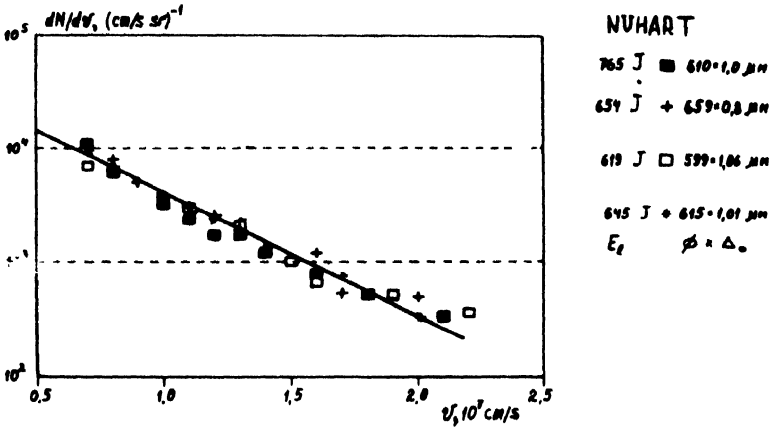

Figure 6. Atom velocity distributions in the nonuniform target irradiation shots (usual conditions) : (1) shell diameter 610 μm, thickness 1.0 μm, E_{las} = 765 J, $Y_n = 3 \times 10^9$; (2) 659 × 0.8 μm, 654 J, 1.5×10^9; (3) 599 × 1.06 μm, 619 J, 2×10^9; (4) 615 × 1.01 μm, 645 J, 1.5×10^9.

where N_0 is equal to 10^5 (cm/s×sr)$^{-1}$, v_0 is equal to 0.3 cm/s. All these shots were performed with nonuniform shell irradiation and high neutron yields (1.5 – 3)×10^9 per shot were registered. Note, that all the spectra exhibit rather high level of atoms with velocities less than 1×10^7 cm/s. This feature is emphasized by Figure 7, which demonstrate atom spectrum of small shell (diameter 497 μm) and high laser energy (770 J). We may consider this shot as example of influence of target support stalk and conclude that the slowest spectrum part may be produced by it. Another origin of slow atoms may be connected with strong mixing effect in the moment of implosion and microshell decay.

In Figure 8 the spectra of uniform target irradiation shots are presented. In these shots the local laser intensity was lower than in the "hot" spots of nonuniform case, what correlated

with the increased implosion time measured with X-ray streak camera and reduced neutron yield $Y_n \approx (0.2\text{-}1.5)\times 10^8$.

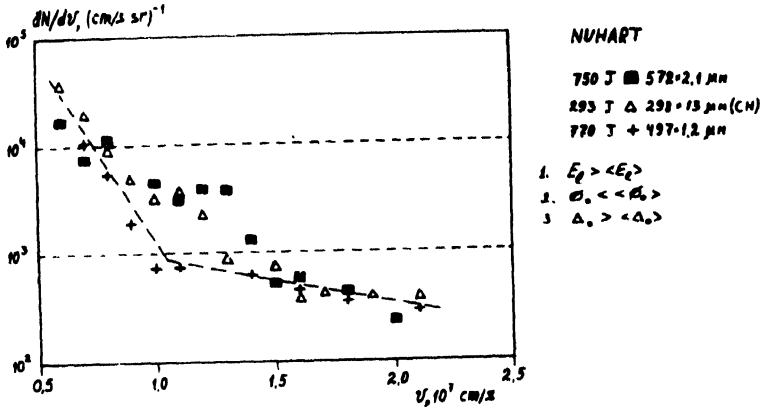

Figure 7. Atom velocity distributions in the high laser intensity shots : (1) 572 × 2.1 μm, 750 J, empty SiO_2 shell, (2) 497 × 1.2 μm 770 J 1.5×10^8, 298 × 13 μm, 293 J, empty CH shell

Atom velocity distributions have maxima around $v = 1\times 10^7$ cm/s. We can explain decreasing of slow atom number ($v \leq 1\times 10^7$ cm/s) by weak influence of target stalk at lower local laser flux and by more spherical implosion without mixing and shell destruction. In the range of velocities $v > 2\times 10^7$ cm/s the number of atoms is less than for the nonuniform case too. This phenomenon can be understood, if one take into account geometry of atom observation. Instead of "cold" area in uniform case we registered fast atoms from plasma with higher temperature and higher ion charge. Besides that, reduction of fast atoms' number may indicate the absence of cumulative streams in the observation direction as was shown by Golulev *et al* [18].

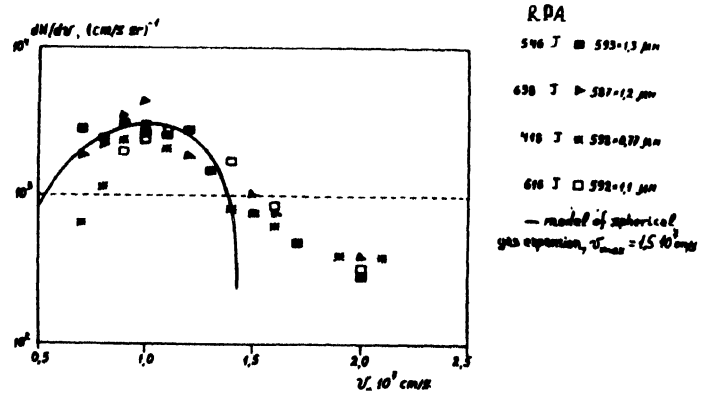

Figure 8. Atom velocity distributions in the uniform target irradiation shots : (1) 593 × 1.3 μm, 546 J, 2.1×10^7; (2) 587 × 1.2 μm, 638 J, 3.9×10^7 (3) 598 × 0.77 um, 418 J, 1×10^8; (4) 592 × 1.1 μm, 616 J, 1.5×10^8 (5) approximation with expanding gas sphere model.

Comparison of Figure 6 and Figure 8 results in the following conclusion : only uniform irradiation case can be analysed for the residual target mass investigation, nonuniform irradiation is associated with obscuring effects of stalk emittance, mixing, target destruction and recombination in low temperature and low ion charge plasma corona.

Comparison of numerical simulation with experiment :

Looking for the common features in numerical and experiment atom distributions one can notice similarity of velocity ranges and rough equality of total atom numbers (within factor of order for var. # 1). Main difference is the broadening of the experimental spectrum. This probably indicate on intensive shell-fuel mixing in the periods of shell deceleration and initial phase of expansion, when conditions for Rayleigh-Taylor instability at the interface between two target parts of different densities realised (lighter fluid accelerates the heavier fluid).

In our earlier work [10] we proposed the simple model for description of this phase — expansion of homogeneous recombining ball in the vaccum. Numerical solution of the process was obtained and it was noted that inclusion of recombination does not influence strongly on the expansion dynamics. Therefore for the first approximation, it is possible to use self consistent solution for adiabatic expansion of gas ball into the vacuum [19] :

$$\frac{dN}{dv} = \frac{N_0}{v_m}\left(\frac{v}{v_m}\right)^2\left[1-\left(\frac{v}{v_m}\right)^2\right]^{1/(\gamma-1)} \tag{4}$$

where v_m is maximal velocity, γ is adiabatic exponent, value of N_0 is determined by normalising integration. The graph of this function is presented in Figure 8 ($N_0 = 5\times10^3$, $V_m = 1.5\times10^7$ cm/s).

It is important to note obvious defect of the model, which does not account the deceleration of the shell debris in the surrounding plasma corona. In the Figure 5 density peaks are propagated in plasma region. They are formed by expanded shock waves in plasma corona, so some part of kinetic energy of residual microshell mass transform to the external plasma layer. In spite of low density of plasma corona considerable deceleration of shell debris is occurred. That is why final atom velocity is less than maximal implosion velocity (u_s).

Shell deceleration effect become clear if simplified model of elastic interaction of two objects with masses M_s (shell) and m_p (plasma) is applied. Let u_s and v_{p1} are the initial velocities of shell and plasma, respectively (v_p is associated with plasma mass centre). Momentum transferred to plasma in the interaction is

$$\Delta I = M_s(u_s - u_n) = M_p\left(v_{p_2} - v_{p_1}\right), \tag{5}$$

where u_n is shell velocity after deceleration (velocity of neutral atom mass centre). We can estimate final plasma velocity, assuming that $v_{p_1} \approx c_s$ – plasma speed,

$$v_{p2} = c_s + u_n \left(\frac{M_s}{M_p} \left(\frac{u_s}{u_n} - 1 \right) \right) \tag{6}$$

Using conservation of kinetic energy in elastic collision it is possible to obtain from (6)

$$\frac{M_s}{M_p} = \frac{(u_s + u_n - c_s)}{(u_s - u_n)} \tag{7}$$

and

$$v = u_s + u_n - c_s \tag{8}$$

In the discussed experiments implosion velocity was determined with X-ray streak imaging and usually was equal to $(2.5 - 3)\times 10^7$ cm/s, and we can use it as u_s. Registered average atom velocity was $u_n \approx 1\times 10^7$ cm/s. Plasma sonic speed for these experiments was in the range $c_s = (1 - 1.5)\times 10^7$ cm/s. So from (7) and (8) we get $M_p = (0.5 - 1)\ M_s$ and $v_{p2} = (2–3)\times 10^7$ cm/s.

Pressure pulse, transferred into the plasma, propagates through the decreasing density profile and shock front acceleration occurs. In Afanasiev *et al*'s work [20], similar density peaks in plasma corona were observed with interferometry. It is possible that just this front was registered by neutral particle detector (Figure 2a) as fast atoms with velocities $(3\text{-}4)\times 10^7$ cm/s. According to (8) shock velocity v_{p2} in plasma increases with decreasing of c_s (this is especially valid for "cold" plasma region in the observation direction) and may considerably exceed u_n (and even velocity u_s). On the contrary, under the uniform irradiation case v_{p2} approaches the u_n, and simultaneously neutral atom number in the "hot" plasma is decreased because of higher average ion charge.

In should be noted that two-peaked structure of ion and neutral particle signals, observed in Figure 2a, can be produced in the result of two-dimensional effects development under nonuniform microshell heating and compression. At the qualitative level we can give following explanation of the feature.

In Figure 9, the scheme of target irradiation is shown. Ablation pressure at the axis of laser beam due to higher intensity is higher than at the bisector of the angle between adjoining beams. So at the shell implosion phase "hot" spots accelerate to the higher velocities and produce convex shock fronts in the fuel gas volume. After implosion reflected shocks are formed and temperature (as well as sound speed) increase very fast, large pressure gradients tend to smooth itself in nonspherical imploded shell. Such conditions are very favourable for cumulative jet initiating in the "cold" area of the shell, because of it arriving delay to the centre. When cumulation is occurred some part of cold unablated shell obtain additional momentum in the direction close to the observation angle. It is possible that the second peak on the ion and the first peak on neutral particle signals belong to the cumulated target material. This assumption is correlated with fact of reduction of these signals in the uniform irradiation shots (see Figure 2b). The second peak on the neutral particle signal corresponds to the shell

and fuel debris, imploded in the microshell centre. For quantitative description of the imploded target expansion process as a whole, it is necessary to conduct two-dimensional numerical simulations, and at present corresponding mathematical model is now being work out.

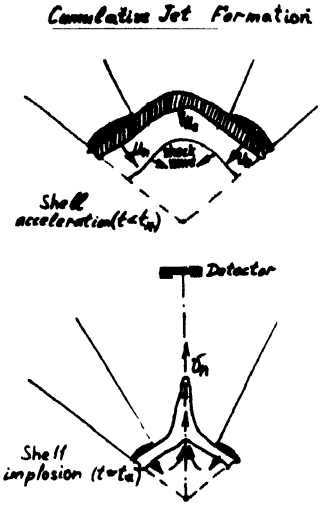

Figure 9. The scheme of cumulative jet formation along bisector of the angle between laser beams axis, Broken line represent the collapsing front, arrows show the direction of resulting pressure gradient and acceleration of target debris.

5. Conclusion

The numerical simulation analysis of ion and atom expansion velocity spectra made possible to distinguish between different components, appeared from laser imploded shell targets in two variants of laser beams focusing. Emission measurements and source images of neutral particles from high aspect ratio shell targets were found to be useful as a sensitive method of controlling the uniformity of implosion.

Comparison of experimental data with the numerical results revealed the effect of momentum transfer from expanding target debris to the plasma corona and the formation of density peak, propagated down the plasma density gradient. Velocity of this peak can be experimentally measured and used as diagnostics of implosion conditions.

It should be specially noted that the diagnostic techniques tested in these experiments can be successfully applied to experiments with ablative mode of shell implosion.

References

[1] N G Basov, Yu A Zakharenkov, N N Zorev, A A Rupasov, G V Sklizkov and A S Shikanov 1986 *Heating and Compression of Thermonuclear Targets by Laser Beam* (Cambridge : Cambridge University Press)

[2] Yu V Afanasiev and V B Rozanov 1972 *JETP* **62** 247

[3] Yu A Bykovskiy, N N Degtyarenko, V S Fetisov *et al.* 1974 *J. Tech. Phys.* **44** 73

[4] R R Goforth and P Hammerling 1976 *J. Appl. Phys.* **47** 3918

[5] G J Tallents 1980 *Tallents, Plasma Phys.* **2** 709

[6] Yu A Bykovskiy and S M Silnov 1989 *Sov. Phys. Plasma* **15** 1091

[7] N G Basov, Yu A Zakharenkov, A A Rupasov, G V Sklizkov and A S Shikanov 1989 *Deuse Plasma Diagnostics* (Moscow : Nauka)

[8] H Hora 1981 *Physics of Laser Driven Plasmas* (New York : John Wiley)

[9] S Denus, J Farny, M Grudzien *et al* 1986 *Laser and Particle Beams* **Vol 4** pt 3,4 507

[10] Yu A Zakharenkov, A A Kaĭnavkhov, V Ya Karpv *et al* 1988 *Sov Phys. Plasma Phys.* **14** 623

[11] C N Danson 1989 *Annual Report to the Laser Facility Committee* **RAL-89-045** 133

[12] M J Lamb, M Savage and P Lews *et al* 1990 *20th Europ Conf Laser Interaction with Matter,* Schlixrsee, Jan, 22-26

[13] M H Key, M J Lamb, A P Fews *et al* 1989 *Opt. Commun.* **71** 184

[14] Z Ahmad, A A Erokhin, Yu A Zakharenkov *et al* 1990 *JETP Lett* **51** 553

[15] A A Erokhin, Yu A Zakharenkov, A A Karnaukhov *et al* 1989 *Sov Phys Plasma Phys* **15** 1076

[16] N V Zmitrenko, V Ya Karpov, A P Fadeev *et al* 1983 *Methods and Programs for Numerical Solving of Mathematical Physics Problems* **Vol. 2** p 38 (In Russian)

[17] A A Golubev, Yu A Zakharenkov, A A Karnaukhov *et al* 1988 *Quant. Electronics* **15** 630

[18] E E Gable, B H Failor, C V Armentrout *et al* 1989 *Phys Rev Lett* **63** 2737

[19] Ya B Zeldovich and Yu P Raizer 1966 *Physics of Shock Waves and High Temperature Hydrodynamic Phenomena* (New York Academic)

[20] Yu V Afanasiev, N G Basov, B L Vasin *et al* 1979 *JETP* **77** 2539